Journal of Statistical Physics, Vol. 64, Nos. 3/4, 1991

Monte Carlo Simulation of Many-Arm Star Polymers in Two-Dimensional Good Solvents in the Bulk and at a Surface

Kaoru Ohno[1,2] **and Kurt Binder**[2]

Received February 7, 1991

A Monte Carlo technique is proposed for the simulation of statistical properties of many-arm star polymers on lattices. In this vectorizing algorithm, the length of each arm l is increased by one, step by step, from a starting configuration with $l=1$ or $l=2$ which is generated directly. This procedure is carried out for a large sample (e.g., 100,000 configurations). As an application, we have studied self-avoiding stars on the square lattice with arm lengths up to $l_{\max}=125$ and up to $f=20$ arms, both in the bulk and in the geometry where the center of the star is adsorbed on a repulsive surface. The total number of configurations, which behaves as $\mathcal{N} \sim l^{\gamma_g-1}\mu^l$, where $\mu=2.6386$ is the usual effective coordination number for self-avoiding walks on the square lattice, is analyzed, and the resulting exponents $\gamma_g=\gamma(f)$ and $\gamma_s(f)$ for the bulk and surface geometries are found to be compatible with predictions of Duplantier and Saleur based on conformal invariance methods. We also obtain distribution functions for the monomer density and the distance of the end of an arm from its center. The results are consistent with a scaling theory developed by us.

KEY WORDS: Monte Carlo simulation; polymer; star polymer; polymer network; self-avoiding walk; two dimensions; critical exponent; surface adsorption; radial distribution function; total number of configurations.

1. INTRODUCTION

The statistical property of star polymers in dilute solution of a good solvent have been finding increasing attention recently: simulations,[1-3] extrapolation of exact enumerations,[4-7] scaling theories,[8-17] and renormalization group analyses[10,15-21] have been applied. Properties of star

[1] Institute for Materials Research, Tohoku University, Katahira, Aoba-ku, Sendai 980, Japan.
[2] Institut für Physik, Universität Mainz, Staudinger Weg 7, W-6500 Mainz, Germany.

0022-4715/91/0800-0781$06.50/0

polymers with a large number $f \gg 1$ of arms is not only an interesting theoretical issue, but of practical interest, since polymers with such an "architecture" have in fact been synthesized[22] and the theoretical concepts possibly apply also to structures such as micelles.[23]

The static properties of star polymers that have been mainly considered are the total number of configurations $\mathcal{N}$ and various structural characteristics. For a polymer network of some general topology $\mathcal{G}$ consisting of f flexible linear chains having all the same length l, $\mathcal{N}_l$ behaves as

$$\mathcal{N}_l \sim l^{\gamma_{\mathcal{G}}-1}\mu^{fl} \tag{1.1}$$

where for a lattice model μ describes an "effective coordination number" for the self-avoiding-walk (SAW) problem: e.g., $\mu = 2.6386$ on the square lattice.[4-7] The associated exponent $\gamma_{\mathcal{G}}$, however, depends on the topological structure of the polymer network.[10,16] In particular, for a star polymer in the bulk this exponent $\gamma_{\mathcal{G}} = \gamma(f)$ depends on the number of arms, while different exponents $\gamma(f)$ result if the center of the star is adsorbed on a wall[7,16] or if one arm end $[\gamma_1(f)]$ or two ends $[\gamma_{11}(f)]$ are adsorbed at the wall[7,16] (Fig. 1).

Structural quantities of interest are the mean square distance between the end (E) of an arm and the center (C) (cf. Fig. 2)

$$R_{\mathrm{CE}} = \langle (\mathbf{r}^{\mathrm{CE}})^2 \rangle^{1/2} = \left\langle \frac{1}{f} \sum_{\substack{\text{endpoints} \\ i=1}}^{f} (\mathbf{r}_i^{\mathrm{E}} - \mathbf{r}^{\mathrm{C}})^2 \right\rangle^{1/2} \tag{1.2}$$

and the corresponding distribution function $g(r^{\mathrm{CE}})$, as well as the mean square radius of gyration

$$R_{\mathrm{gyr}} = \left\langle \frac{1}{N} \sum_{j}^{N} (\mathbf{r}_j - \mathbf{r}^{\mathrm{CG}})^2 \right\rangle^{1/2} \tag{1.3}$$

and the mean square distance from the center

$$R_{\mathrm{C}} = \left\langle \frac{1}{N} \sum_{j}^{N} (\mathbf{r}_j - \mathbf{r}^{\mathrm{C}})^2 \right\rangle^{1/2} \tag{1.4}$$

and the radial density distribution function $g(r)$ around the center of the star. In Eqs. (1.2)–(1.4), $N = fl$ is the total number of monomers which are at positions $\{\mathbf{r}_j\}$ in a considered configuration, $\langle \cdots \rangle$ means an average over all configurations, and $\mathbf{r}^{\mathrm{C}}$, $\mathbf{r}^{\mathrm{CG}}$, and $\mathbf{r}_i^{\mathrm{E}}$ denote the positions of the star center point, its center of gravity, and the end of the ith arm, respectively. Equations (1.2)–(1.4) all refer to a star polymer in the bulk (Fig. 1a)—for

star polymers in surface-adsorbed geometries (Figs. 1b, 1c) the directions parallel and perpendicular to such a repulsive wall are not equivalent, of course, and then certain generalizations of Eqs. (1.2)–(1.4) are appropriate, as will be discussed in the next section.

Now both enumeration techniques[4–7] and the renormalization group expansion in $\varepsilon = 4 - d$[10,15–21] are very difficult to apply for large f: exact enumerations only work if $\mathcal{N}$ is not too large and thus for large f the accessible arm lengths l get too small for a meaningful extrapolation to

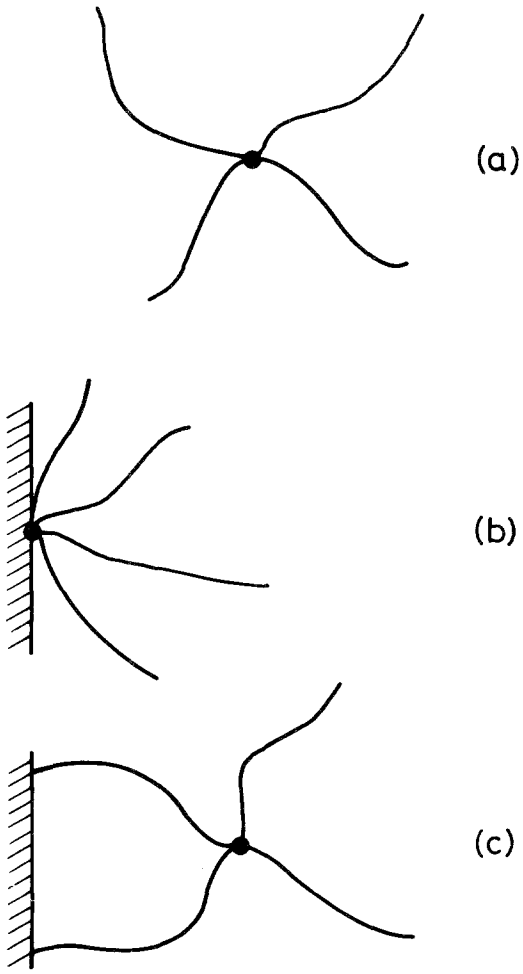

Fig. 1. Three topologies of a 4-arm star: (a) the free star in solution in the bulk, (b) the center-adsorbed star, and (c) the star with two arm ends being adsorbed.

$l \to \infty$; in the ε-expansion, the expansion parameter is εf rather than ε itself, and hence for $f \to \infty$ additional approximations are required.[21] Thus it is very desirable to study such problems by computer simulation. While the molecular dynamics technique is capable of dealing with many-arm star polymers,[1,2] it does not yield information on the number of configurations and hence it cannot estimate exponents such as $\gamma(f)$, $\gamma_s(f)$, $\gamma_1(f)$, $\gamma_{11}(f)$,

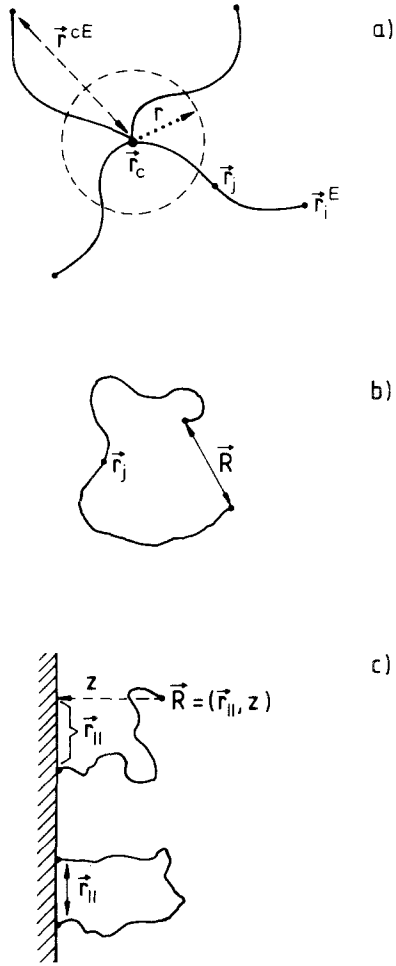

Fig. 2. Notation of distances in (a) a star polymer and (b) a linear polymer in the bulk and (c) with one or two ends adsorbed at the surface. Each arm has l monomers (labeled by an index j, at a position $\mathbf{r}_j$). The radial distance of a monomer from the star center is denoted by r. The end-to-end distance of a linear polymer is denoted by $\mathbf{R}$. In the surface-adsorbed geometry, distances perpendicular to the wall (z) and parallel to it ($\mathbf{r}_{||}$) need to be distinguished.

etc. While this problem in principle should be accessible by biased sampling methods,[3] biased sampling always involves subtle accuracy problems.[24]

Thus in the present paper we propose a new Monte Carlo method for the simulation of many-arm star polymers utilizing a completely stochastic (unbiased) sampling (Section 3). As an application, we study star polymers with arm lengths up to $l=125$ and number of arms up to $f=20$ on the square lattice, generating typically 60,000 samples with a vectorizing algorithm on various supercomputers. In Section 4, the resulting properties of free stars in the bulk are described and compared to the results by Duplantier,[10] which were obtained by conformal invariance methods and hence are believed to be exact, and thus provide a crucial test for our methods. In Section 5, results for center-adsorbed star polymers at surfaces are presented, and compared to the corresponding (presumably exact) results of Duplantier and Saleur.[11] Section 6 contains our conclusions and outlook for future work.

2. A SURVEY OF PERTINENT THEORETICAL PRECICTIONS

From the renormalization group expansion in $\varepsilon=4-d$, the following structure for the exponents $\gamma(f)$, $\gamma_s(f)$ has emerged[16]:

$$\gamma(f)=1+(\gamma-1)\left[f-\frac{f(f-1)}{2}\right]+f(f-1)(f-2)\,A(f) \tag{2.1}$$

$$\gamma_s(f)=1+(\gamma_1-1)f-(\gamma_{11}+\nu)\frac{f(f-1)}{2}+f(f-1)(f-2)\,B(f) \tag{2.2}$$

Here $A(f)$ and $B(f)$ are polynomials of both ε and f and are of order ε^2; $A(f)$ has been found[16,21] as $\varepsilon^2/64+\mathcal{O}(\varepsilon^3)$. The exponents γ, γ_1, γ_{11}, and ν characterize linear polymers in the bulk and at a surface, respectively: the mean square end-to-end distance behaves as

$$\langle R^2\rangle \sim l^{2\nu} \tag{2.3}$$

where $\nu=3/4$ for $d=2$,[25] and the number of configurations is

$$\mathcal{N} \sim l^{\gamma-1}\mu^l \tag{2.4}$$

$$\mathcal{N}_1 \sim l^{\gamma_1-1}\mu^l \tag{2.5}$$

and

$$\mathcal{N}_{11} \sim l^{\gamma_{11}-1}\mu^l \tag{2.6}$$

for free chains (Fig. 2b) and chains adsorbed with one end ($\mathcal{N}_1$) or both ends ($\mathcal{N}_{11}$) at the wall (Fig. 2c), respectively.[26]

As f increases, $\gamma(f)$ has been conjectured to behave as[21] $\gamma(f) \sim -f^{d/(d-1)}$. For $d=3$ dimensions, the accuracy of the expansion to order ε^2 in Eq. (2.1) is only good for small f, as a comparison to the presumably more accurate Monte Carlo data[3] shows. For $d=2$ dimensions, on the other hand, it is believed that the following formulas are exact[10,11]:

$$\gamma(f) = \frac{17}{16} + \frac{9}{32}\left[f - \frac{f(f-1)}{2}\right] \tag{2.7}$$

$$\gamma_s(f) = 1 + (\gamma_1 - 1)f - (\gamma_{11} + \nu)\frac{f(f-1)}{2} = 1 + \frac{15}{64}f - \frac{9}{32}f^2 \tag{2.8}$$

and also the exponents γ, γ_1, γ_{11} are believed to be known exactly[25,27] in $d=2$, $\gamma = 43/32$, $\gamma_1 = 61/64$, and $\gamma_{11} = 3/16$. It is interesting to note that Eq. (2.8) has the form of Eq. (2.2) with $B(f)=0$, while Eq. (2.7) is not consistent with Eq. (2.1). The reason for this latter discrepancy is still unclear.

Now the exponents $\gamma_{11\ldots1}(f)$ for star polymers with f arms out of which g are adsorbed with their ends on the surface are given in terms of the simple scaling relation[16]

$$\gamma_{11\ldots1}(f) = \gamma(f) + \nu + g[\gamma_{11} - \gamma_1] \tag{2.9}$$

Next we consider the quantities R_{CE}, R_{gyr}, and R_C characterizing the structure of the polymer [Eqs. (1.2)–(1.4)]. Now the scaling theories[8–16] imply that

$$R_C \sim R_{gyr} \sim R_{CE} \sim l^{\nu} \tag{2.10}$$

Any f dependence can show up only in the prefactor in these relations which should scale proportional to $f^{(1-\nu)/(d-1)}$.[8] Equation (2.10) also holds if the center and/or some arm ends are adsorbed at the surface.[16] However, considerably more interesting are the various radial distribution functions. A recent scaling theory predicts for the monomer density function[17]

$$\rho(\mathbf{r}) = \frac{1}{r^{d-1/\nu}}\psi\left(\frac{r}{R_C}\right) \tag{2.11}$$

and for the center-end distribution function

$$g(\mathbf{r}^{CE}) = \frac{1}{R_{CE}^d} \phi\left(\frac{r^{CE}}{R_{CE}}\right) \tag{2.12}$$

Here the short-distance behavior of these scaling functions $\psi(x)$ and $\phi(x)$ has been obtained as[18]

$$\psi(x) \sim 1 \tag{2.13}$$

$$\phi(x) \sim x^{\theta(f)} \tag{2.14}$$

where the exponent $\theta(f)$ is given by[17]

$$\theta(f) = [\gamma - \gamma(f+1) + \gamma(f) - 1]/\nu \tag{2.15}$$

In the case of the center-adsorbed star, these functions depend on the parallel distance $r_{||}$ and the perpendicular distance from the wall (z) separately[17]

$$\rho_s(\mathbf{r}_{||}, z) = N(R_C)^{-d} \psi_s\left(\frac{r_{||}}{R_C}, \frac{z}{R_C}\right) \tag{2.16}$$

$$g_s(\mathbf{r}_{||}^{CE}, z^E) = (R_{CE})^{-d} \phi_s\left(\frac{r_{||}^{CE}}{R_{CE}}, \frac{z^E}{R_{CE}}\right) \tag{2.17}$$

The short-distance behavior of these quantities has been predicted as[17]

$$\rho_s(r_{||}, 0) \sim r_{||}^{-d+\lambda(f)} \tag{2.18}$$

$$\rho_s(0, z) \sim z^{-d+1/\nu} \tag{2.19}$$

$$g_s(\mathbf{r}_{||}^{CE}, 0) = (r_{||}^{CE})^{\theta_{||}(f)} \tag{2.20}$$

$$g_s(0, z^E) = (z^E)^{\theta_\perp(f)} \tag{2.21}$$

where the exponents $\lambda(f)$, $\theta_{||}(f)$, and $\theta_\perp(f)$ have been derived as follows[17]:

$$\lambda(1) = 0, \qquad \lambda(f) = 1/\nu \quad \text{for} \quad f \to \infty \tag{2.22}$$

$$\theta_{||}(f) = [\gamma_1 - \gamma_s(f+1) + \gamma_s(f) - 1]/\nu \tag{2.23}$$

$$\theta_\perp(f) = [\gamma - \gamma_s(f+1) + \gamma_s(f) - 1]/\nu \tag{2.24}$$

3. MONTE CARLO ALGORITHM

While "dynamic" algorithms such as the bond fluctuation method[28] would be suitable to obtain structural properties [such as considered in Eqs. (1.2)–(1.4), (2.10)–(2.21)], they cannot yield estimates for the number

of configurations and associated exponents γ_{sg} [Eqs. (1.1), (2.1)–(2.9)]. While the latter quantities could in principle be obtained from standard simple sampling,[29] a straightforward application of this technique for many-arm star polymers would fail due to the well-known "attrition problem"[29]: the success rate of growing an f-arm star of arm length l decreases exponentially as $(\mu/3)^{fl} \approx (1.137)^{-Nl}$, on the square lattice. However, this problem can be overcome by a simple modification of the simple random sampling. Suppose we have a sample of M_l configurations of an f-arm star polymer with given l (l is the length of each arm), and want to utilize this sample for making one-step larger star polymers, i.e., stars with the arm-length $l+1$. On a square lattice, there are three ways of elongating one end of an arm by one unit, if we discard the fourth direction where the arm would fold backward on itself, which is forbidden for self-avoiding polymers. Thus, in growing an f-arm star polymer, there would be 3^f ways of elongating the ends of the f arms by one unit (some of which also would have to be discarded because of the self-avoidance condition). Thus, if we would want to consider all possible realizations at the $(l+1)$th step from M_l distinct realizations at the lth step, we would have to make $3^f M_l$ trials and discard all unphysical realizations which violate the self-avoidance condition. Of course, this number $3^f M_l$ would be prohibitively large for large values of f. However, it is not necessary to consider all possible $3^f M_l$ trial configurations: it is enough to consider a stochastically chosen sample mM_l of them, where $m \ll 3^f$ for large f. The size of this sample must be chosen so large that the number M_{l+1} of the configurations which are accepted out of the mM_l trial configurations, i.e., those which do not violate the self-avoidance condition, are of the same order of M_{l+1}, since now the process can be iterated: $M_l \approx M_{l+1} \approx M_{l+2} \approx \cdots$, starting out for $l=3$, say, since configurations for $l=1$ and $l=2$ usually can be generated differently (e.g., from exact enumeration). Since the expected number M'_{l+1} of accepted configurations out of the full number of trial configurations $3^f M_l$ is

$$\frac{M'_{l+1}}{M_l} = \frac{\mathcal{N}_{l+1}}{\mathcal{N}_l} = \mu^f \tag{3.1}$$

and since the actual number of trial configurations made is mM_l instead of $3^f M_l$, we can also conclude

$$\frac{M_{l+1}}{M_l} = \frac{M'_{l+1}}{M_l}\frac{m}{3^f} = m\left(\frac{\mu}{3}\right)^f \tag{3.2}$$

We see that the condition $M_{l+1}/M_l \approx 1$ is satisfied if we choose $m \approx (3/\mu)^f \approx (1.137)^f$. Even for f as large as $f=20$, a rather small value of m (≈ 13) results. In practice for small l it is better to work with somewhat

larger values of m; in any case, this type of "enrichment algorithm" for star polymers is practically applicable.

From Eqs. (1.1), (3.1), and (3.2) we see that the precise value of the ratio M_{l+1}/M_l yields the desired information on the exponent γ_g, since

$$\frac{\mathcal{N}_{l+1}}{\mathcal{N}_l} = \frac{3^f M_{l+1}}{m M_l} = \mu^f \left\{ 1 + \frac{\gamma_g - 1}{l} + \mathcal{O}\left(\frac{1}{l^2}\right) \right\} \tag{3.3}$$

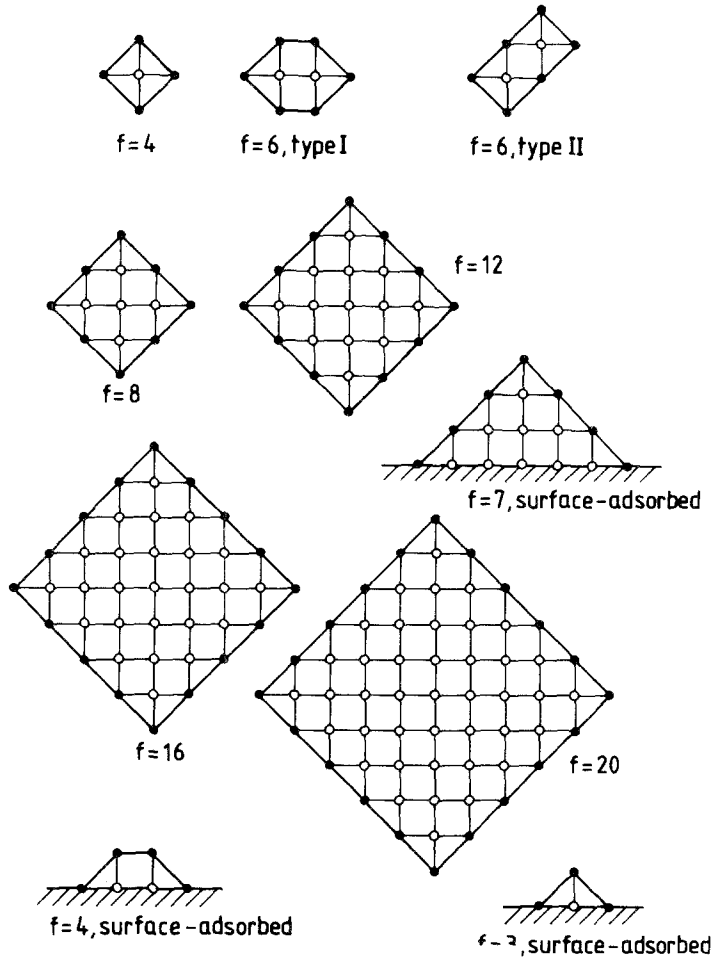

Fig. 3. Core regions of the star polymers simulated in the present paper. Each black dot is the center point of a single arm which is grown starting from this point. While for the number of arms $f = 4$, 8, 12, 16, and 20 the core is always a regular diamond shape, for other values of f less regular shapes result, and one can consider several types of shapes for the same value of f, as indicated for $f = 6$.

Consequently, the configuration number exponent $\gamma(f)$ [or $\gamma_s(f)$, respectively] is determined from a plot of $3^f M_{l+1}/(mM_l)$ versus $1/l$: if the numerical data fall on a straight line with the (known) intersection μ^f on the ordinate axis, the slope of this straight line yields $[\gamma_g - 1]\,\mu^f$.

At this point, we make a comment about the center of the star

(a)

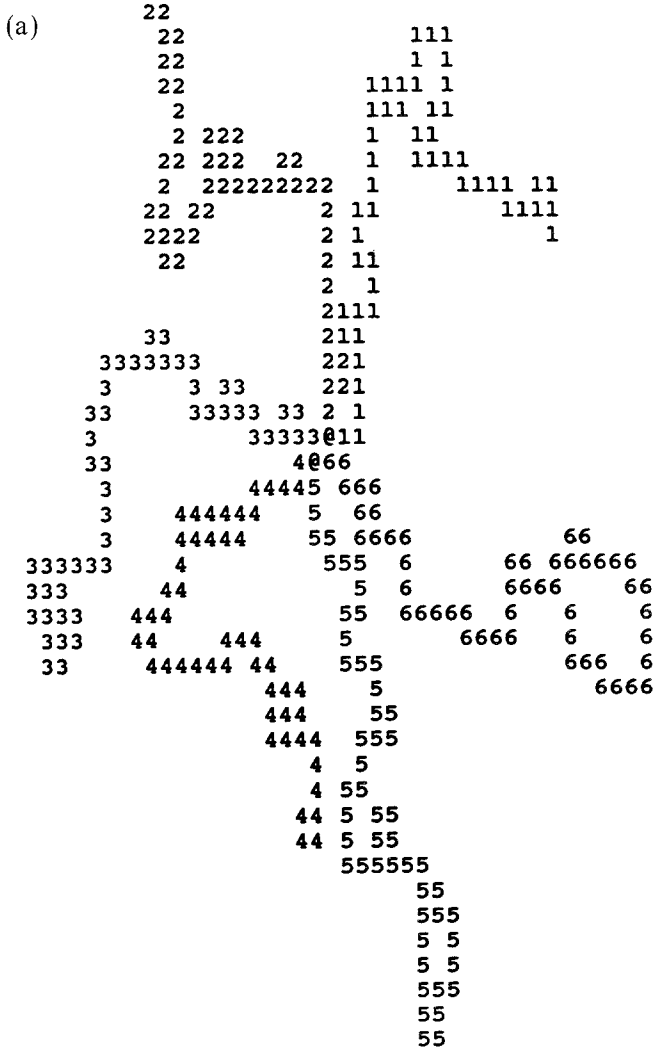

Fig. 4. Typical configurations of a (a) type II 6-arm star and (b) a center-adsorbed 4-arm star. The symbols @ denote the sites in the inner part of the core region (denoted by open circles in Fig. 3), while the positions of the monomers of each arm are indicated by printing the label i of each arm at the corresponding position. Both cases refer to $l = 50$.

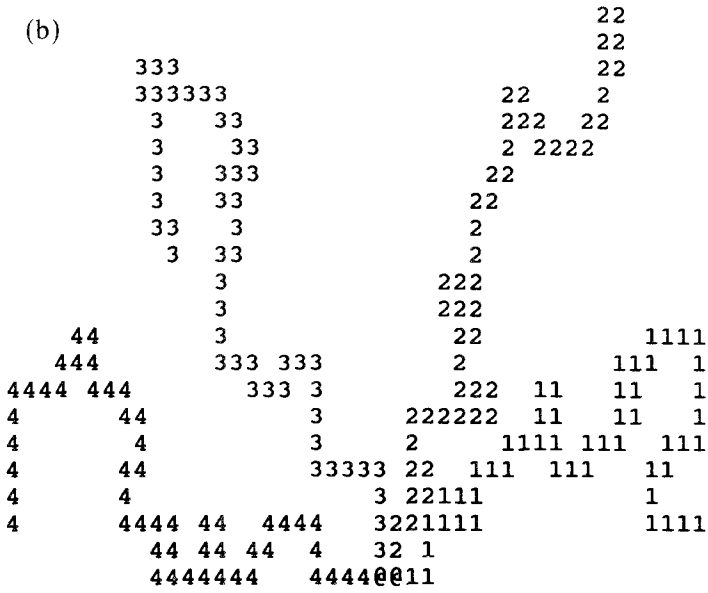

Fig. 4. (*Continued*)

polymer. If one requires the center to be a lattice point, obviously $f \leqslant q$, where q is the coordination number of the lattice ($q=4$ here). Being interested in larger f values, more extended core regions in the center of the star must be admitted. The choice of the precise size and slope of this core region involves some inevitable ambiguity. Figure 3 shows the core regions of star polymers used in the actual simulations. In order to avoid too dense configurations near the center of the star (which might give rise to a rather slow approach to the limiting behavior considered here), we choose relatively large cores such that already for $l=1$ a large number of configurations exists. On the other hand, it is clear that for observation of truly asymptotic behavior it may be necessary that the relevant distances which are considered are much larger than the linear dimensions of the star core. Obviously, this region is not at all easy to reach for large f. The present paper thus does not really aim at deriving very precise exponent estimates, but rather intends to demonstrate the feasibility of the approach and test its strengths as well as its weaknesses. Therefore we have confined ourselves also to a relatively modest investment of computer time: Choosing $M_l=2000$ for $2 \leqslant l \leqslant 9$, $M_l=20{,}000$ for $10 \leqslant l \leqslant 19$, and $M_l=60{,}000$ for $20 \leqslant l \leqslant 50$, the program for $f=4$, 8, 12, 16, and 20 took altogether about 10 hours in CPU time on a NEC SX-2 supercomputer to estimate $\gamma(f)$, reaching a vectorization percentage of 97.8%. For a study of the distribu-

tion functions $g(r^{CE})$ and $\rho(r)$ and for the study of surface-adsorbed polymers additional runs were performed (using up to $M_l = 150{,}000$ and l up to $l_{max} = 125$ on a Siemens-Fujitsu VP100 computer, using altogether about 10 hours in CPU time). As an example of the "raw data" thus generated, Fig. 4 shows "snapshot pictures" of a "type II" 6-arm star in the bulk, and a $f = 4$ surface-adsorbed star.

4. NUMERICAL RESULTS FOR FREE STARS IN THE BULK

If we make a direct plot of $\mathcal{N}_{l+1}/\mathcal{N}_l$ [estimated from recording the set $\{M_l\}$ and using Eq. (3.3)] versus $1/l$, for various values of f separately, in order to estimate $\gamma(f)$ (typically Fig. 5 shows such a curve for $f = 12$), we generally find that the curvature on the plot vs. $1/l$ is the stronger the larger f, and this observation clearly suggests that the asymptotic region has not been reached in a naive sense. The increased size of the core, Fig. 3, which is a region "blocked" for the arms, systematically reduces the number of configurations for short arm length; such an effect is not unexpected. This means there is a correction to scaling to the leading asymptotic behavior in Eq. (1.1). Another, rather trivial effect results from the problem that for large f the absolute value of the exponent $\gamma_g - 1 = \gamma(f) - 1$ in Eq. (1.1)

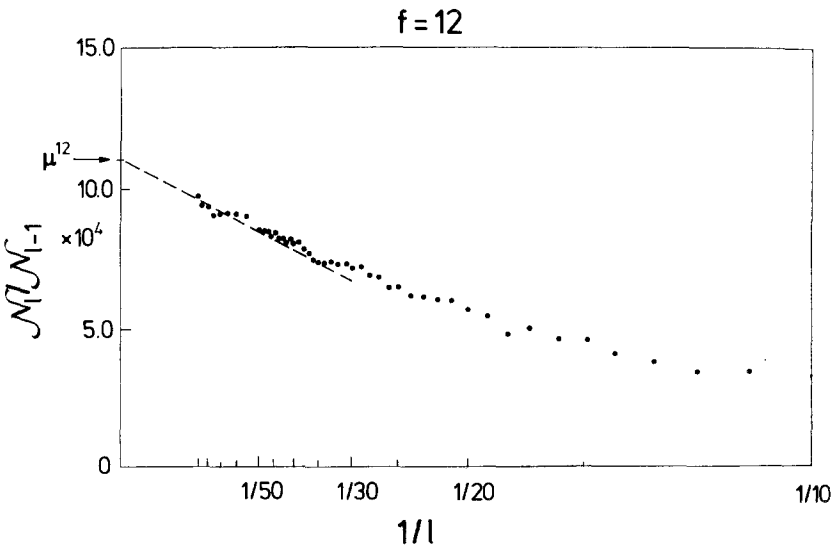

Fig. 5. Plot of $\mathcal{N}_l/\mathcal{N}_{l-1}$ versus $1/l$ for 12-arm stars ($f = 12$). Arrow on the ordinate shows μ^f, while the broken straight line is a tentative fit to the data. Here $l \leqslant l_{max}$ with $l_{max} = 90$.

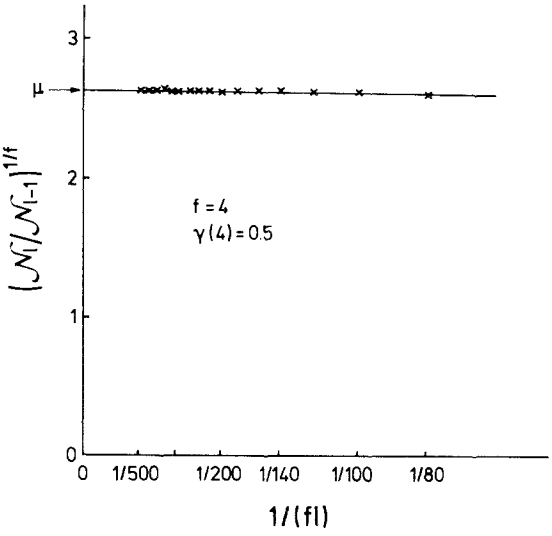

(a)

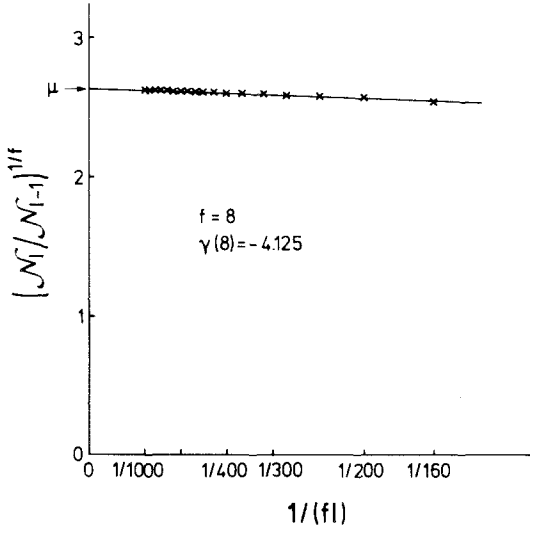

(b)

Fig. 6. Plot of $(\mathcal{N}_l/\mathcal{N}_{l-1})^{1/f}$ versus $1/l$ for (a) 4-arm stars, (b) 8-arm stars, (c) 12-arm stars, (d) 16-arm stars, and (e) 20-arm stars. Arrow on the ordinate shows $\mu = 2.6386$, while the straight line is the best fit to the data. Note that $l \leqslant l_{\max}$ with $l_{\max} = 125$ (for $f = 4, 8$), $l_{\max} = 90$ (for $f = 12$), and $l_{\max} = 50$ (for $f = 16, 20$).

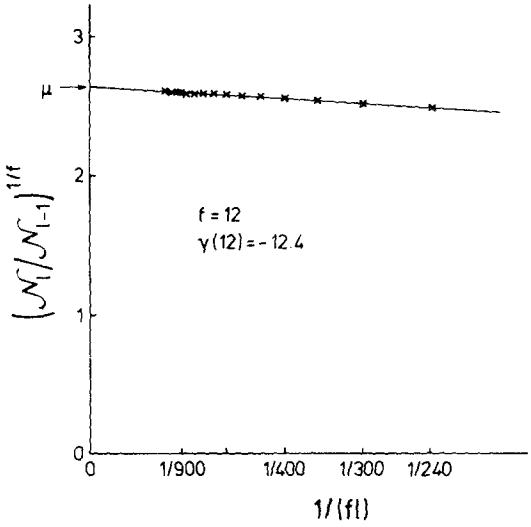

(c)

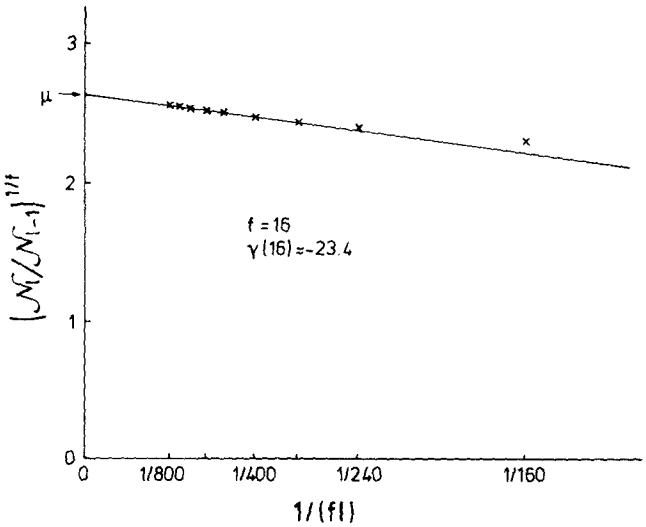

(d)

Fig. 6. (*Continued*)

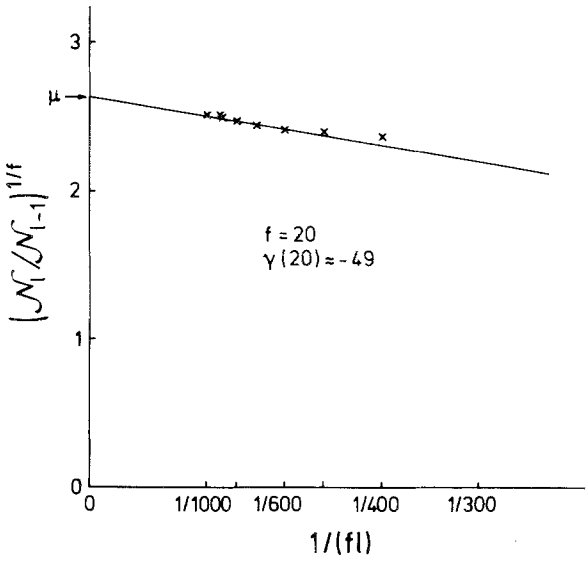

(e)

Fig. 6. (*Continued*)

is so large. Assuming there were no correction terms to Eq. (1.1), the binomial expansion taken one order higher than Eq. (3.3) yields

$$\frac{N_{l+1}}{N_l} = \mu^f \left\{ 1 + \frac{\gamma_g - 1}{l} + \frac{[\gamma_g - 1][\gamma_g - 2]}{2l^2} + \cdots \right\} \tag{4.1}$$

which shows that the quadratic correction in Eq. (3.3) is negligible only for $l \ll |\gamma(f) - 2|/2$; such an asymptotic regime has not been reached clearly for large f. This problem can be reduced by rather considering a plot of $(\mathcal{N}_{l+1}/\mathcal{N}_l)^{1/f}$ versus $1/fl$, since now

$$\left(\frac{N_{l+1}}{N_l}\right)^{1/f} = \mu \left\{ 1 + \frac{\gamma_g - 1}{fl} + \frac{[\gamma_g - 1][\gamma_g - 1 - f]}{2(fl)^2} + \cdots \right\} \tag{4.2}$$

i.e., the quadratic correction is negligible for $l \gg |\gamma(f) - 1 - f|/(2f)$, which is always reached with our data. Replotting our data according to Eq. (4.2) removes most of all curvature, showing that corrections to scaling are now relatively small. Figure 6 shows the plot of $(\mathcal{N}_l/\mathcal{N}_{l-1})^{1/f}$ versus $1/fl$ for $f = 4$, 8, 12, 16, and 20. The asymptotic value $\mu = 2.6386$ is shown on the ordinate and the slope of the resulting "best fit" straight lines gives our estimates of $\mu[\gamma(f) - 1]$. A phenomenological recipe to remove the rest

Table I. Comparison of Our Best Estimates for $\gamma(f)$ and $\gamma_s(f)$ with the Corresponding Exact Results (2.7) and (2.8)

f	$\gamma(f)$ estimated	$\gamma(f)$ exact
4	0.5 ± 0.1	$1/2 = 0.5$
8	-4.1 ± 0.5	$-73/16 = -4.5625$
12	-14 ± 1	$-113/8 = -14.125$
16	-28 ± 4	$-451/16 = -28.1875$
20	-46 ± 6	$-374/8 = -46.75$
f	$\gamma_s(f)$ estimated	$\gamma_s(f)$ exact
3	-0.8 ± 0.1	$-53/64 = -0.828$
7	-10 ± 1	$-713/64 = -11.141$
11	-28 ± 4	$-1949/64 = -30.453$

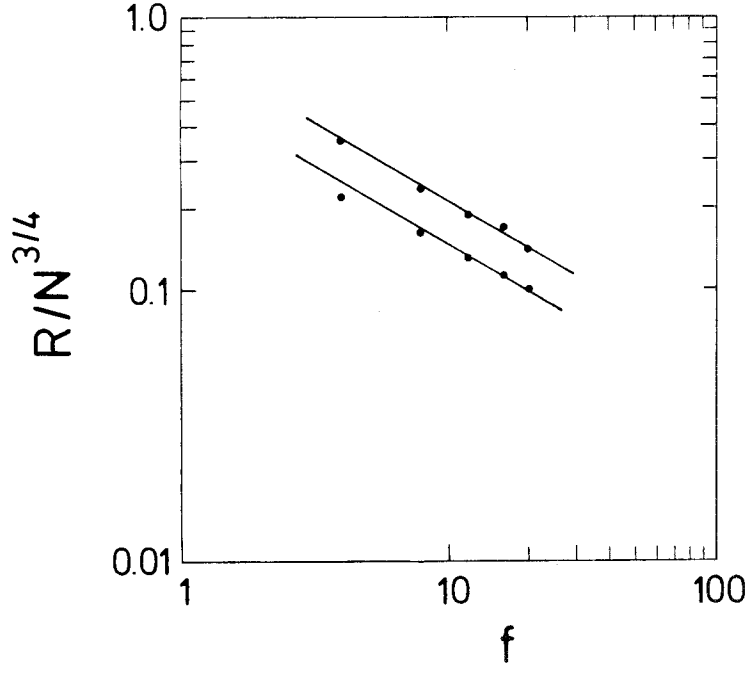

Fig. 7. Log-log plot of $R/N^{3/4}$ for $l = 50$ plotted vs. f, where R is the center-end distance R_{CE} (upper set of data points) and the mean distance from the center R_C (lower set). Straight lines indicate the Daoud–Cotton prediction, $R/N^{3/4} \sim f^{1/2}$.

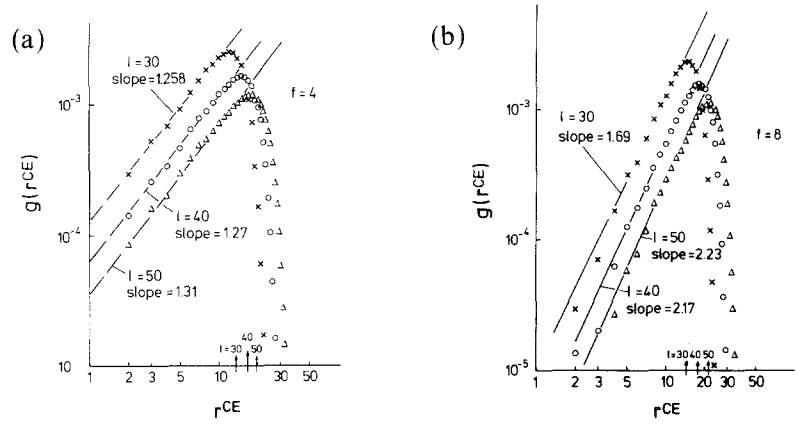

Fig. 8. Log-log plot of the end-center distribution function $g(r^{CE})$ vs. r^{CE} for (a) $f=4$ stars and (b) $f=8$ stars. $g(r^{CE})$ is normalized as $\sum_{\mathbf{r}} g(\mathbf{r})=f$, and data shown are for $l=30$ (crosses), $l=40$ (circles) and $l=50$ (triangles), respectively. The arrows in the abscissa show the respective estimates of R_{CE}. Straight lines indicate the behavior $g(r^{CE}) \sim (r^{CE})^{\theta^{eff}(f)}$. The effective exponents $\theta^{eff}(f)$ are quoted in Table II. All these data were based on 90,000 samples.

curvature on this extrapolation plot is to plot $(\mathcal{N}_l/\mathcal{N}_{l-1})^y$ versus $1/l$, where for each f the appropriate exponent y is adjusted to yield the best straight line fit. However, the strong statistical scatter of our data hardly warrants such a procedure. Table I quotes our best estimates obtained from these fitting procedures, together with Duplantier's exact result. For all the

Table II. Comparison of the Effective Exponents Observed for $l=50$ in the Monte Carlo Simulation for the Center-End Distribution Function with the Corresponding Exact Results Using Eqs. (2.7), (2.8), (2.15), (2.20)

f	$\theta^{eff}(f)$	$\theta(f)=(2+9f)/24$
4	1.3	$19/12=1.583$
8	2.2	$37/12=3.083$
12	3.3	$55/12=4.583$
16	4.5	$73/12=6.083$
f	$\theta_{\|\|}^{eff}(f)$	$\theta_{\|\|}(f)=3f/4$
3	1.9	$9/4=2.25$
7	3.9	$21/4=5.25$
f	$\theta_{\perp}^{eff}(f)$	$\theta_{\perp}(f)=(25+36f)/48$
3	1.7	$133/48=2.771$
7	3.8	$277/48=5.771$

values of f the agreement is satisfactory within the error of estimates, although for $f \geqslant 12$ the accuracy of the present simulation clearly is too limited to be able to obtain significant exponent estimates.

In spite of these limitations, our data do allow a significant study of linear dimensions such as R_C and R_{CE} [Eqs. (1.2), (1.4)]. Figure 7 checks the Daoud–Cotton scaling by plotting R_C/N^ν and R_{CE}/N^ν vs. f, to check the predicted[8] variation as $f^{\sigma-\nu}$, where $\sigma = (1-\nu)/(d-1) = 1/4$ in $d=2$. The data are in good agreement with this prediction.

Next we consider the center-end distribution function. Figure 8 shows typical data for (a) 4-arm stars and (b) 8-arm stars. It is seen that these data are in fact consistent with a power-law description for $r^{CE} < R_{CE}$ as assumed in Eq. (2.14). However, one has to be careful: the slope of the straight line systematically increases with increasing arm length l, which indicates that one sees an effective exponent $\theta^{eff}(f)$, and not the true asymptotic exponent $\theta(f)$ given by Eq. (2.15). Table II, which collects all

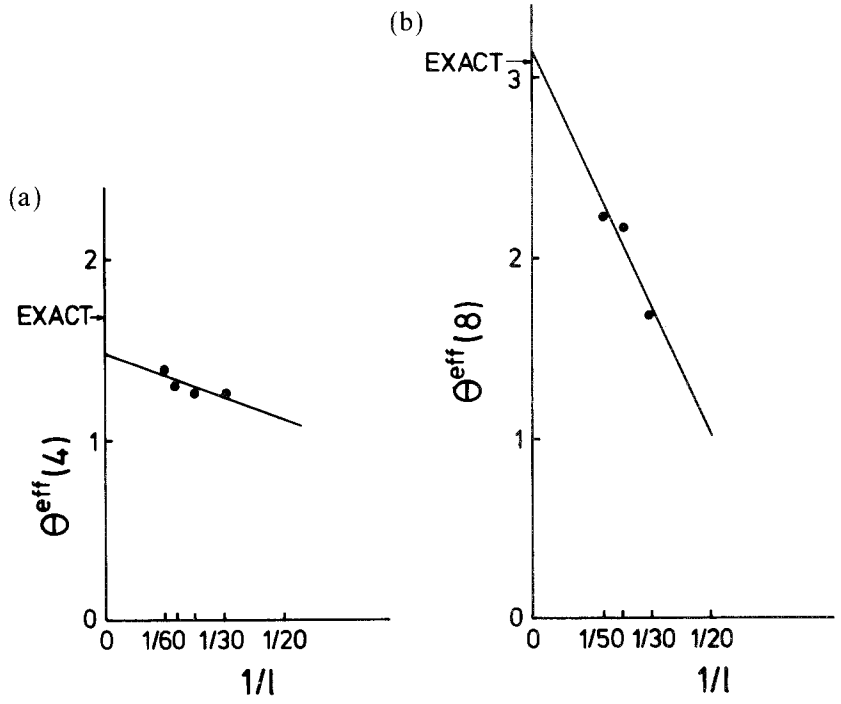

Fig. 9. Extrapolation of $\theta^{eff}(f)$ vs. $1/l$ for (a) 4-arm stars and (b) 8-arm stars. Arrow shows the predicted exact result which follows from the scaling relation, Eq. (2.15), and Duplantier's formula,[10] Eq. (2.7).

such data (including the surface-adsorbed case), shows that these effective exponents (for arm length $l = 50$) are systematically too low, in particular for large f. For obtaining the true asymptotic exponents $\theta(f)$, $\theta^{\text{eff}}(f)$ must be extrapolated as a function of $1/l$ toward $l \to \infty$ (Fig. 9). It is seen that this extrapolated value becomes relatively closer to the exact result, but a very precise estimation of $\theta(f)$ is not possible by such methods. This is a warning against too hasty a conclusion in $d = 3$ dimensions, where no guidance by exact results will be available!

Finally, we turn to the monomer density distribution function $\rho(r)$. As an example, Fig. 10 presents the log-log plots for both types of 6-arm stars included in Fig. 3. The slope of the straight line indicates our estimation of effective exponents: -0.57 for type I (see Fig. 10a) and -0.51 for type II (see Fig. 10b). Only for type II are the data straightforwardly consistent with the correct exponent $1/\nu - d = -2/3$ [Eq. (2.11)], while for larger f the exponent found in the simulation is closer to about -0.6. However, there is also some systematic distinction between the two topologies in Fig. 9, and thus it is clear that the asymptotic regime where the true exponent can be read off has not quite been reached.

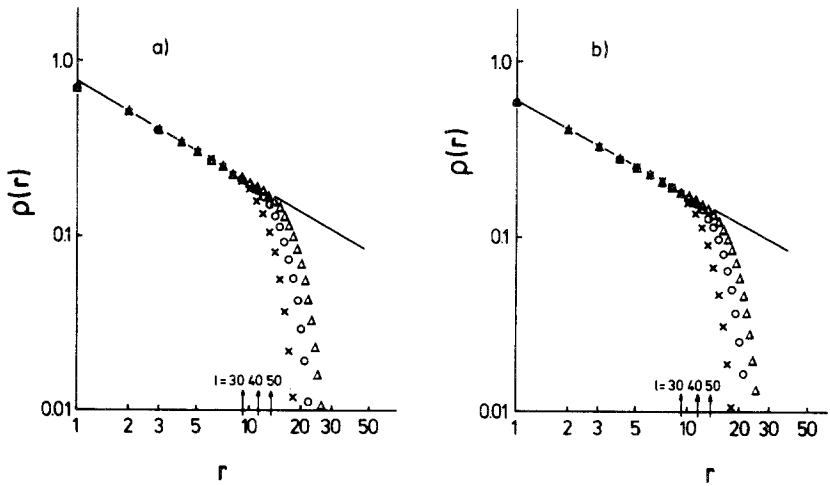

Fig. 10. Log-log plot of the monomer density distribution $\rho(r)$ vs. r, for both topologies, (a) type I and (b) type II, of 6-arm stars. The normalization is chosen such that $\rho(\mathbf{r}) = 1$ if the site $\mathbf{r}$ is occupied. Results for three values of l are plotted in the same figure: $l = 30$ (crosses), $l = 40$ (circles), and $l = 50$ (triangles). The arrows in the abscissa show the respective estimates of R_C. The slope of the straight line is given by -0.57 for type I and -0.51 for type II. Both these sets of data should be compared to the exact value $1/\nu - d = -2/3$.

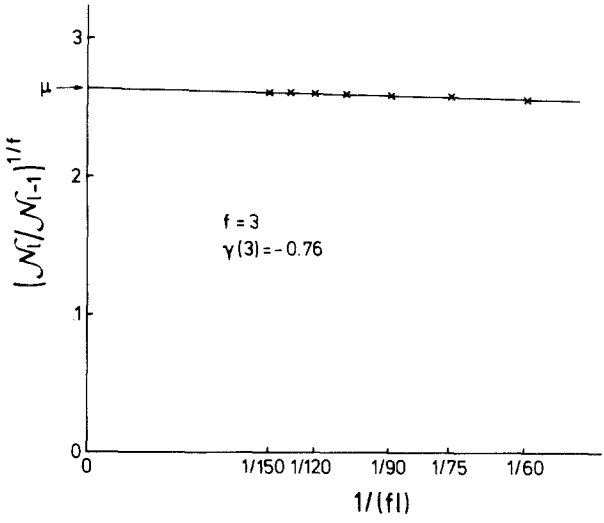

(a)

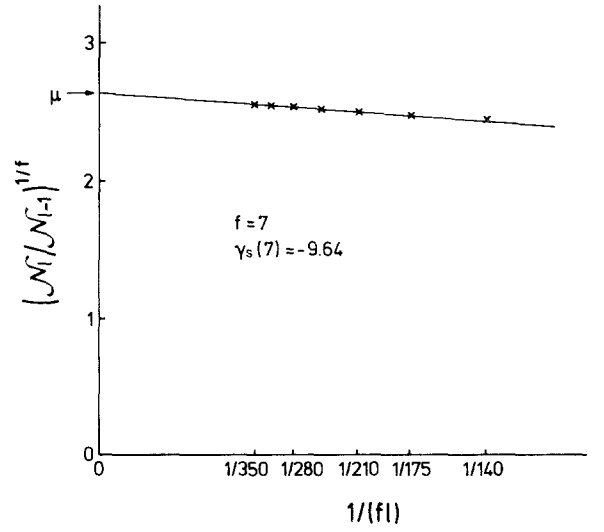

(b)

Fig. 11. Plot of $(\mathcal{N}_l/\mathcal{N}_{l-1})^{1/f}$ versus $1/fl$ for the center-adsorbed (a) 3-arm, (b) 7-arm, and (c) 11-arm star polymers, i.e., for $f = 3$, 7, and 11. Arrow on the ordinate shows $\mu = 2.6386$, while the straight line is the best fit to the data. The arm lengths are rather short, $l \leqslant l_{\max}$ with $l_{\max} = 50$, but data seem already in the scaling regime.

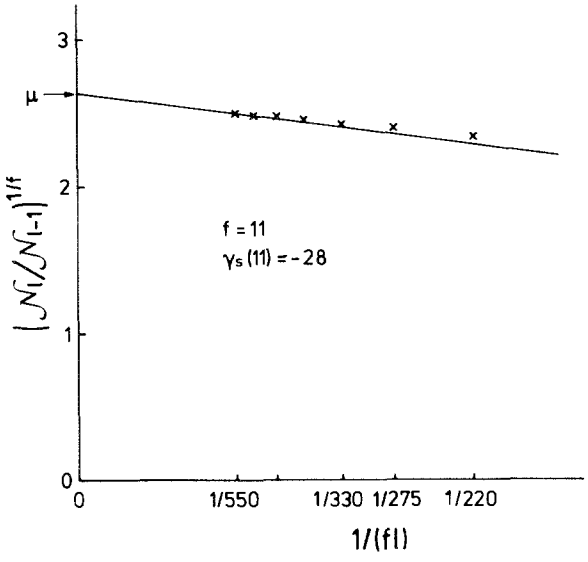

(c)

Fig. 11. (*Continued*)

5. NUMERICAL RESULTS FOR SURFACE-ADSORBED STAR POLYMERS

Figure 11 shows a plot of $(\mathcal{N}_l/\mathcal{N}_{l-1})^{1/f}$ versus $1/fl$ for $f=3$, 7, and 11. The asymptotic value $\mu=2.6386$ is shown on the ordinate and the slope of the resulting "best fit" straight lines gives our estimates of $\mu[\gamma(f)-1]$. Table I quotes our best estimates obtained from these fitting procedures, together with Duplantier's exact results. For all the values of f the agreement is satisfactory within the error of estimates, although for $f=11$ the accuracy of the present simulation clearly is too limited to be able to obtain significant exponent estimates.

Also in this center-adsorbed case, we examine linear dimensions R_C and R_{CE} [Eqs. (1.2), (1.4)]. According to the cone picture,[21] or a simple generalization of the Daoud–Cotton theory,[8] these variables for the center-adsorbed stars should have the same behavior as the free stars. Figure 12 plots R_C/N^ν and R_{CE}/N^ν vs. f, to check the expected variation as $f^{\sigma-\nu}$, where $\sigma=(1-\nu)/(d-1)=1/4$ in $d=2$. The data are in good agreement with this expectation.

Next we consider the center-end distribution function $g(r_{||}^{CE}, z^E)$. Figure 13 shows typical data for (a) 3-arm stars and (b) 7-arm stars. It is

seen that these data are in fact consistent with a power-law description for $r^{CE} < R_{CE}$ as assumed in Eqs. (2.20) and (2.21). However, the slope of the straight line systematically increases with increasing arm length l, which indicates that one sees effective exponents $\theta_{||}^{eff}(f)$, $\theta_{\perp}^{eff}(f)$ and not the true asymptotic exponents $\theta_{||}(f)$, $\theta_{\perp}(f)$ given by Eqs. (2.23) and (2.24). Table II collects all such data. Again, for obtaining the true asymptotic exponents $\theta(f)$, $\theta^{eff}(f)$ must be extrapolated, for example, as a function of $1/l$ toward $l \to \infty$. It is seen that this extrapolated value becomes closer to the exact result, but a very precise estimation of $\theta(f)$ is not possible by such methods.

Finally we turn to the monomer density distribution function $\rho(r_{||}, z)$. As an example, Fig. 14 presents a result for the 4-arm center-adsorbed stars included in Fig. 3. The slope of the straight line indicates our estimation of effective exponents: $a = -1.4 \pm 0.3$ for $\rho(r_{||}, 0) \sim r_{||}^{a}$ and $b = -0.62 \pm 0.05$ for $\rho(0, z) \sim z^{b}$. For the exponent $\lambda(f)$ defined in Eq. (2.18) we have $\lambda(4) = a + b = 0.7 \pm 0.3$, although the error of estimates is still quite large [this

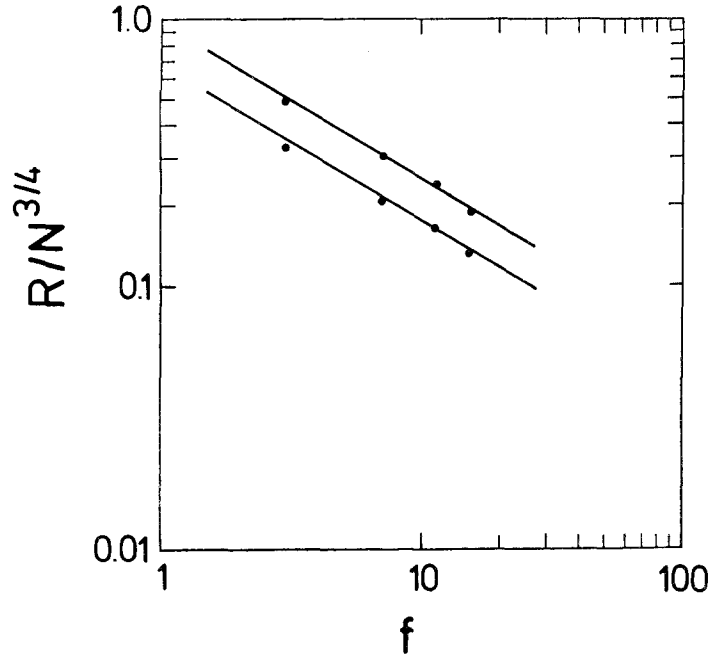

Fig. 12. Log-log plot of $R/N^{3/4}$ for $l = 50$ plotted vs. f in the case of center-adsorbed stars, where R is the center-end distance $R_{CE,||} \simeq R_{CE,\perp}$ (upper set of data points) and the mean distance from the center $R_{C,||} \simeq R_{C,\perp}$ (lower set). Straight lines indicate the theoretical slope, $R/N^{3/4} \sim f^{1/2}$.

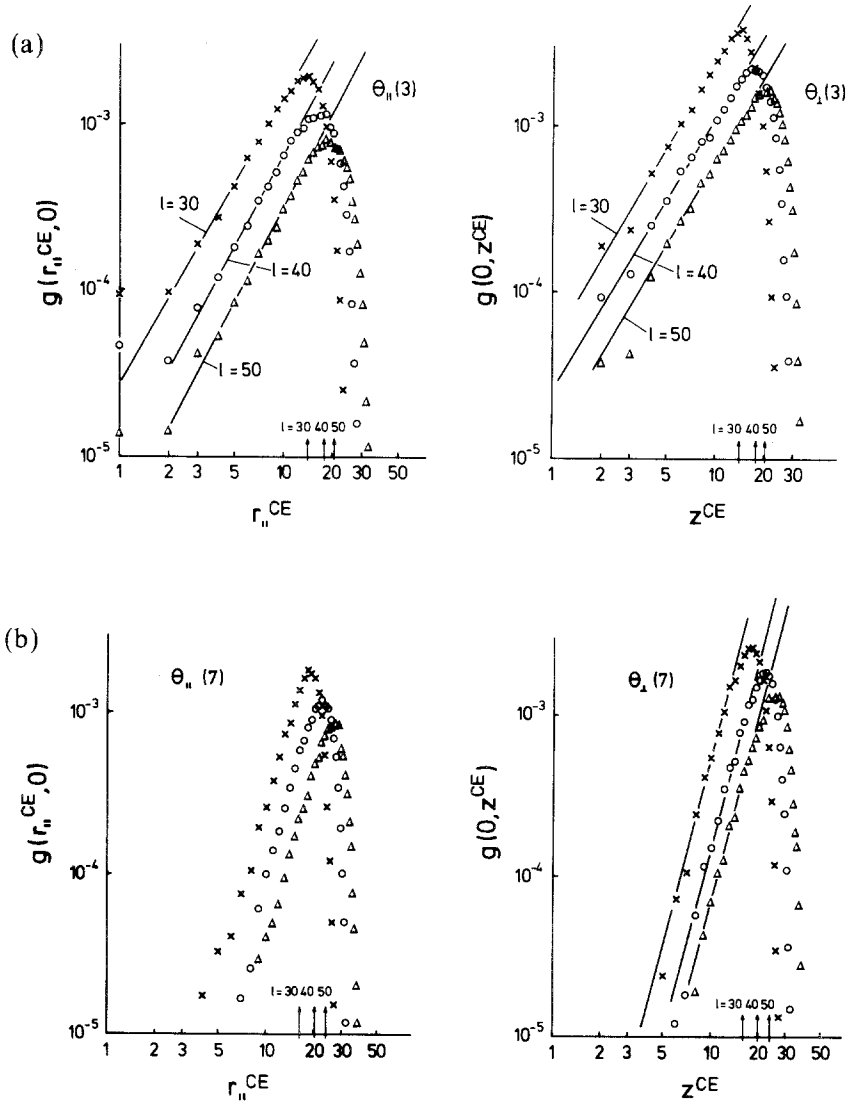

Fig. 13. Log-log plot of the center-end distribution functions. The plots of $g(r_{\|}^{CE}, 0)$ vs. $r_{\|}^{CE}$ (left figure) and $g(0, z^{CE})$ vs. z^{CE} (right figure) are given, respectively, for (a) 3-arm stars and (b) 7-arm stars. Note that $z^{CE} = z^{E}$ in the text. $g(r^{CE})$ is normalized as $\sum_{\mathbf{r}} g(\mathbf{r}) = f$, and data shown are for $l = 30$ (crosses), $l = 40$ (circles), and $l = 50$ (triangles). The arrows in the abscissa show the respective estimates of $R_{CE,\|} \sim R_{CE,\perp}$. Straight lines indicate the behaviors $g(r_{\|}^{CE}, 0) \sim (r_{\|}^{CE})^{\theta_{\|}^{eff}(f)}$ (left) and $g(0, z^{E}) \sim (z^{E})^{\theta_{\perp}^{eff}(f)}$ (right). The effective exponents $\theta_{\|}^{eff}(f)$ and $\theta_{\perp}^{eff}(f)$ are quoted in Table II. These data for $f = 3$ and $f = 7$ were based on 150,000 samples and 100,000 samples, respectively.

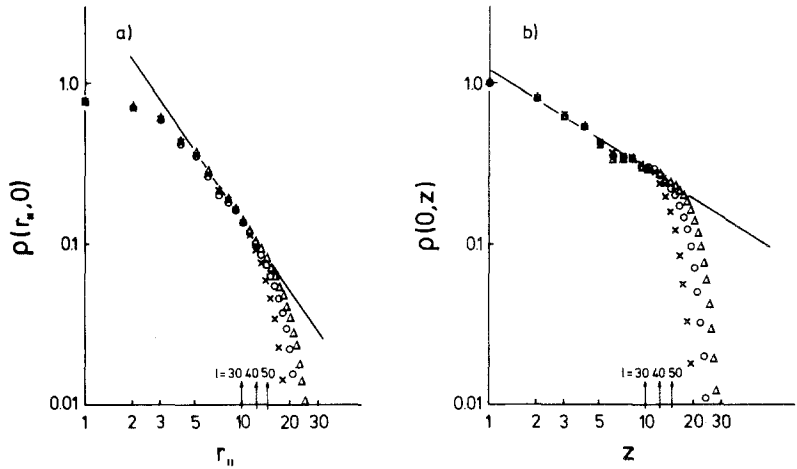

Fig. 14. Log-log plot of the monomer density distribution for the center-adsorbed star polymers with $f=4$: (a) the plots of $\rho(r_{\|}, 0)$ vs. $r_{\|}$, (b) the plots of $\rho(0, z)$ vs. z. The normalization is chosen such that $\rho(\mathbf{r})=1$ if the site $\mathbf{r}$ is occupied. Data shown include various arm lengths l, i.e., $l=30$ (crosses), $l=40$ (circles), and $l=50$ (triangles). The arrows in the abscissa show the respective estimates of $R_{C,\|} \simeq R_{C,\perp}$. The slope of the straight line indicates estimation of effective exponents: $a=-1.4\pm0.3$ for $\rho(r_{\|}, 0) \sim r_{\|}^{a}$ and $b=-0.62\pm0.05$ for $\rho(0, z) \sim z^{b}$. The exponent b is straightforwardly consistent with the correct exponent $1/\nu - d = -2/3$.

value of the exponent $\lambda(f)$ should be compared with the result of our $\varepsilon = 4-d$ expansion analysis[30]], while the exponent b is straightforwardly consistent with the correct exponent $1/\nu - d = -2/3$ [Eq. (2.19)] within the error of estimates.

6. CONCLUDING REMARKS

In this paper, we have studied the statistical properties of many-arm star polymers in good solvents and two-dimensional geometry, both in the bulk and with the center of the star being adsorbed on a flat (one-dimensional) surface. Modeling the arms of the star as self- and mutually-avoiding walks of l steps on the square lattice (with $l \leqslant l_{\max}=125$), extended cores in the center of the star as shown in Fig. 3 are used in order to be able to treat f-arm stars with f up to $f_{\max}=20$.

Standard Monte Carlo methods for the simulation of self-avoiding walks (or mutually-avoiding walks[31]) cannot be applied to such star polymers without problems. Therefore a variant of a simple sampling method is suggested in this paper and successfully applied. This new method is related in spirit to the "enrichment techniques" well known[32]

for linear polymers. While in standard simple sampling the success rate of growing our f-arm star of arm length l decreases exponentially as $(\mu/3)^{fl}$ where $\mu = 2.6386$ on the square lattice, in our modified method we do not try to add a bond at each arm end of the star once to go from l to $l+1$, but rather we try this m times independently, from all the M_l configurations kept in the lth "generation." Choosing $m \approx (3/\mu)^f = 1.137$, one can (for large f) easily avoid both an "explosive growth" in the number M_l of the configurations as l increases and an exponential decay toward zero.

This technique is practically useful both for estimating the configuration number exponents $\gamma(f)$ and $\gamma_s(f)$ for the bulk and surface-adsorbed star polymers, respectively, as well as for the study of center-end distribution functions, radial density distribution functions around the center of the star, etc.

We have tested our method by comparing the resulting exponent estimates with presumably exact results due to Duplantier and Saleur. Our estimates for both $\gamma(f)$ and $\gamma_s(f)$ are consistent with these results, but it must be said that at present only a rough accuracy is reached (relative accuracy typically is between 10% and 20% only). Thus our work rather is a feasibility study (and in fact has consumed only a very modest effort of supercomputer time). Unfortunately, a reliable estimation of the exponents $\theta(f)$, $\theta_{||}(f)$, and $\theta_{\perp}(f)$ characterizing the center-end distribution of bulk and surface-adsorbed star polymers seems more difficult: distances r^{CE} much smaller than the radius R_{CE} and much larger than the core diameter are needed, which require distinctly larger l than have been accessible. But the general trend of the "effective exponents" $\theta^{eff}(f)$, $\theta_{||}^{eff}(f)$, and $\theta_{\perp}^{eff}(f)$ observed in our simulations is similar to our previous scaling predictions.

Nevertheless, it seems interesting to try the present method also for three-dimensional star polymers and for cases where other interaction parameters are included (e.g., attractive interactions between monomers or between monomers and the wall, in the center-adsorbed case). It is planned to report on such applications in future work.

ACKNOWLEDGMENTS

One of us (K.O.) is grateful to the Alexander von Humboldt foundation for a fellowship and to Prof. Binder's group in Mainz University for hospitality. Also, support from the Deutsche Forschungsgemeinschaft (DFG), Sonderforschungsbereich 262 is acknowledged. We thank Dr. T. Pakula and Dr. A. Halperin for stimulating and useful discussions.

REFERENCES

1. G. S. Grest, K. Kremer, and T. A. Witten, *Macromolecules* **20**:1376 (1987).
2. G. S. Grest, K. Kremer, S. T. Milner, and T. A. Witten, *Macromolecules* **22**:1904 (1989).
3. J. Batoulis and K. Kremer, *Macromolecules* **22**:427 (1989).
4. J. E. Lipson, S. G. Whittington, M. K. Wilkinson, J. L. Martin, and D. S. Gaunt, *J. Phys. A* **18**:469 (1985).
5. M. K. Wilkinson, D. S. Gaunt, J. E. Lipson, and S. G. Whittington, *J. Phys. A* **19**:789 (1986).
6. A. J. Barrett and D. L. Tremain, *Macromolecules* **20**:1687 (1987).
7. S. A. Colby, D. S. Gaunt, G. M. Torrie, and S. G. Whittington, *J. Phys. A* **20**:515 (1987).
8. M. Daoud and J. P. Cotton, *J. Phys. (Paris)* **43**:531 (1982).
9. T. M. Birshtein and E. B. Zhulina, *Polymer* **25**:1453 (1984).
10. B. Duplantier, *Phys. Rev. Lett.* **57**:941 (1986).
11. B. Duplantier and H. Saleur, *Phys. Rev. Lett.* **57**:3179 (1986); H. Saleur, *J. Phys. A* **19**:L807 (1986).
12. B. Duplantier and H. Saleur, *Phys. Rev. Lett.* **59**:539 (1987).
13. B. Duplantier and H. Saleur, *Nucl. Phys.* **290[FS20]**:291 (1987); B. Duplantier, *Phys. Rev. B* **35**:5290 (1987).
14. B. Duplantier, *Europhys. Lett.* **8**:677 (1988).
15. B. Duplantier, in *Fundamental Problems in Statistical Mechanics, VII*, H. van Beijeren, ed. (Academic Press, New York, 1990).
16. K. Ohno and K. Binder, *J. Phys. (Paris)* **49**:1329 (1988).
17. K. Ohno and K. Binder, *J. Chem. Phys.*, to appear.
18. A. Miyake and K. F. Freed, *Macromolecules* **16**:1228 (1983).
19. A. Miyake and K. F. Freed, *Macromolecules* **17**:678 (1984).
20. C. H. Vlahos and M. K. Kosmas, *J. Phys. A* **20**:1471 (1987).
21. K. Ohno, *Phys. Rev. A* **40**:1524 (1989).
22. K. Huber, W. Burchard, and F. J. Fetters, *Macromolecules* **17**:541 (1984); N. Khasat, R. W. Pennisi, N. Hadjichristidis, and L. J. Fetters, *Macromolecules* **21**:1100 (1988); J. Roovers, P. Tonorowski, and J. Martine, *Macromolecules* **22**:1897 (1989).
23. H. Watanabe and T. Kotaka, *Macromolecules* **17**:342 (1984); L. Leibler and P. A. Pincus, *Macromolecules* **17**:2922 (1984).
24. J. Batoulis and K. Kremer, *J. Phys. A* **21**:127 (1988).
25. B. Nienhuis, *Phys. Rev. Lett.* **49**:1062 (1982).
26. E. Eisenriegler, K. Kremer, and K. Binder, *J. Chem. Phys.* **77**:6296 (1982); see also K. Binder and K. Kremer, in *Scaling Phenomena in Disordered Systems*, R. Pynn and A. Skjeltorp, eds. (Plenum Press, New York, 1985).
27. J. L. Cardy, *Nucl. Phys. B* **240[FS12]**:514 (1984).
28. I. Carmesin and K. Kremer, *Macromolecules* **27**:711 (1988).
29. K. Kremer and K. Binder, *Computer Phys. Rep.* **7**:259 (1988).
30. K. Ohno and K. Binder, *J. Chem. Phys.*, to appear.
31. B. Li and A. D. Sokal, preprint (1990).
32. F. T. Wall and J. J. Erpenbeck, *J. Chem. Phys.* **30**:634, 637 (1959); M. Lax and J. Gillis, *Macromolecules* **10**:334 (1977); C. Brender, D. Ben-Avraham, and S. Havlin, *J. Stat. Phys.* **31**:661 (1983).